Lithological Discrimination and Mapping Using Aster Swir Data in The Tundi Area, Jharkhand

Pratikshya Mishra[1], E.N. Dhanamjaya Rao[2]

[1]Geologist, Geological Survey Of India
[2]Professor, Andhra University

Abstract:

ASTER (Advanced Spaceborne Thermal Emission and Reflection Radiometer) multispectral data is utilized in mineralogical and lithological mapping along with alteration zone mapping. The present study is carried out using ASTER data, which has shown the effectiveness SWIR spectral bands of ASTER data in lithological mapping. Field validation is carried out in the areas where lithological updation was expected from the sspectral analysis. From the band ratios, argillic, ferric, phyllic and propylytic alteration zones were demarcated.

Thus, ASTER SWIR bands coupled with the advanced image enhancement techniques are recommended as a rapid and cost effective tool for lithological discrimination and mapping in the hostile terrain of Dhanbad and other geological areas.

Index Terms: ASTER, Spectral Band Ratio, False Colour Composite , Argillic Alteration, Ferric Alteration, Phyllic Alteration, Propylytic Alteration

I. Introduction

Remotely sensed data can be utilized in varied geological applications such as alteration zone mapping, mineral potential and lithological discrimination [10,38,50,52,54,60]. Landsat Thematic Mapper (TM) and Enhanced Thematic Mapper (ETM+) launched in 1982 and 1999 with 5 and 8 spectral channels are some of the Spaceborn multispectral sensors utilized for such applications[12,52]. Since 2000, Advanced Spaceborne Thermal Emission and Reflection Radiometer (ASTER) multispectral data have been used in mineralogical and lithological studies (Ninomiya, 2002, 2004; Rowan et al., 2003; Rowan and Mars, 2003). The Advanced Spaceborne Thermal Emission and Reflection Radiometer (ASTER) is one of five instruments on the U.S. Terra spaceborne platform (the other instruments are the Moderate Resolution Imaging Spectroradiometer (MODIS), Clouds and the Earth's Radiant Energy System (CERES), Multi-angle Imaging Spectro Radiometer (MISR), and Measurement of Pollution in the Troposphere (MOPITT)). Launched in December 1999, ASTER has been continuously acquiring image data for 20 years. ASTER is a joint project between Japan's Ministry of International Trade and Industry (MITI) (later changed to Ministry of economy, Trade and Industry (METI)) and the U.S. National Aeronautics and Space Administration (NASA) [29].

In 2003, Rowan and Mars were one of the first researchers to report on lithologic mapping using ASTER data, over the rare earth mineral deposit at Mountain Pass, California[45]. Using all 14 ASTER bands, they were able to distinguish calcite from dolomite, mapped skarn deposits and marble in the contact metamorphic zones, distinguished Fe-muscovite from Al-muscovite in the granites and gneisses, and discriminated quartzose rocks. None of these discriminations could be accomplished with Landsat TM data, due to the lack of multispectral SWIR and TIR spectral bands. Watts and Harris[53] applied this method to map granite and gneiss in domes in the Himalayas. Yamaguchi and Naito[57] developed spectral indices using orthogonal transformation with ASTER SWIR bands for lithologic mapping. Their method relied on band ratios and thresholding. Wherever there were good rock exposures, ASTER data produced good results. Analyzing all of the ASTER spectral bands, Byrnes et al.[6] mapped volcanic lava

flows from the Maunu Ulu eruption, Island of Hawaii. The TIR data highlighted variations in the silica coatings, the VNIR and SWIR bands indicated relative ages of the flows as they developed surface weathering products. Gomez et al.[14] published a paper describing lithologic mapping in arid Namibia using ASTER's VNIR and SWIR bands. They first converted the data to apparent reflectance, then processed the data with principal components analysis and supervised classification. Comparison with an existing 1:250,000 scale geologic map indicated that the ASTER data could be used to discriminate most of the geologic units. Several additional units were found, based on compositional differences, though the geologic map defined them as belonging to the same stratigraphic unit. Kargel et al.[25] reviewed applications of ASTER data for glaciological studies. The data were used to distinguish differences in surface cover on top of glaciers, as well as the extent of glacial lakes.

One of the first applications of ASTER TIR data for lithologic mapping was published by Ninomiya et al.[32]. They developed mineralogical indices using blended ratios of the TIR bands to create a Quartz Index, Carbonate Index, and Mafic Index; then tested their technique over arid parts of northwest China, eastern central Australia, and southern Tibet. Their results demonstrated the stability of the mineral indices to temperature and atmospheric changes. In succeeding years, many projects used Ninomiya "indices" for lithologic mapping with ASTER TIR data. More quantitative analyses of ASTER TIR data were reported by Hook et al.[20], who determined weight percent silica in igneous rocks, and validated the findings with laboratory measurements of field samples. About the same time, Rowan et al.[46] reported on lithologic mapping of ultramafic rocks with ASTER data in Mordor Pound, NT, Australia. Analysis of the data, coupled with lab measurements, showed dominantly Al-OH and ferric-iron VNIR–SWIR absorption features in felsic rock spectra, and ferrous-iron and Fe, Mg-OH features in the mafic–ultramafic rock spectra. ASTER ratio images, matched-filter, and spectral-angle mapper processing were evaluated for mapping the lithologies. Combining analyses of VNIR, SWIR and TIR data resulted in discrimination of four mafic–ultramafic categories; three categories of alluvial–colluvial deposits; and a significantly more completely mapped quartzite unit than could be accomplished by using either data set alone. Hewson et al.[19] described a method to seamlessly mosaic 35 ASTER scenes to produce a regional mosaic for analysis. They then mapped Al-OH and carbonate from SWIR data, and quartz content from TIR data. SWIR bands were also used to map Al-OH composition. Comparison with large-scale maps and airborne hyperspectral data, supplemented with field sampling, constrained the ASTER map accuracy. Qiu et al.[38] compared several spectral classification techniques, using a laboratory spectral library, ground spectral measurements, or selecting end members from the image. In the Allaqi-Heiani suture, Egypt, they found all three methods fairly similar, and allowed successful mapping of the well-exposed lithologies. Mapping carbonates and associated rocks in Oman was published by Rajendran et al.[41] and Rajendran and Nasir [42]. They were able to separate the ophiolitic rocks, carbonates, quartz-rich silicates, and surficial deposits. The remote sensing maps were very similar to the published geologic maps, and they recommended using ASTER data for mapping in other, similar environments. Guha et al.[16] also mapped carbonates, using ASTER data for the Kolkhan limestone in India. They applied different spectral mapping techniques; the results were similar with each of them. Yajima and Yamaguchi[56] used simple color composites of TIR data to separate mafic-ultramafic rocks (such as gabbro, dolerite and dunite) from various quartz-rich felsic rocks (such as granite and alluvium). This is a simple method to display lithological information from the TIR bands. Ninomiya and Fu[31] applied Ninomiya indices (Quartz Index, Mafic Index, and Carbonate Index) for ASTER TIR data to do lithological mapping in Tibet. Mapping relied on classification of quartzose rocks based on variations on the carbonate and mafic indices, and the granitic rocks based on the feldspar content. ASTER data were applied to characterize limestones for industrial rock resource assessment in Oman by Rajendran et al.[43]. They were able to separate dolomite from calcite-bearing marble; this has a direct application in the industrial rock business. Several studies focused on mapping granitoid rocks. Massironi et al.[28], working in the Saghro massif, Morocco, used all the ASTER bands, applying simple processing techniques. They were able to distinguish different granitoid rocks with similar silica content based on secondary minerals, and separate plutons with varying silica content

using TIR data. Bertoldi et al.[5] used field and laboratory data to guide processing of ASTER data to map lichen-covered granitic rocks in the western Himalayas. Their maps were based on characterizing spectral differences from various lichens, with spectral characteristics of muscovite. In the Dahab Basin, Egypt, Omran et al.[33] used band ratios of ASTER VNIR, SWIR, and TIR data, combined with field investigations, to map and separate granitoid rocks of Cambrian and Cretaceous ages. They revised and updated existing geologic maps by adding rock units and re-interpreting the geologic history. Zheng and Fu[59] used band ratios of

ASTER SWIR and TIR data to separate alkali-feldspar granite, granite, granodiorite, and monzogranite. These distinctions relied on determination of silica difference expressed in the TIR bands. Advanced Spaceborne Thermal Emission Reflection Radiometer (ASTER) has three spectral bands in the Visible/near Infrared (VNIR) region, six spectral bands in the Shortwave Infrared (SWIR) region and five spectral bands in the Thermal Infrared (TIR) region with 15m, 30m and 90m spatial resolution which can provide a new prospective of investigating earth's surface material for various applications[10,12,47,54]. ASTER data is most suitable for geological applications because of the enhanced resolutions, high Signal to Noise Ratio (SNR), the effective spectral coverage and global data availability. The three spectral bands of ASTER play an important role in various geological applications such as the VNIR region provides spectral features of transition metals such as iron, SWIR region is very effective for analyzing spectral characteristics of carbonate, hydrate and hydroxide minerals, and TIR region is effective for characterization of silicates[7,11]. These three spectral bands help in the identification of hydrothermal alterations such as propylitic, argillic, phyllic and potassic zone[4,36,37,40]. To obtain the lithological, mineral and hydrothermal alteration maps with reasonable accuracies, various image enhancement techniques have been well employed on ASTER datasets[10,13,21,36,37,38,58].

In this study, focus has been emphasized on application of PCA, MNF and on ASTER SWIR data to discriminate the various lithological units. The objective of the present study is to demonstrate the utility of ASTER SWIR data for lithological discrimination and mapping in the Tundi area, Jharkhand.

II. Location and geological setting of the study area

The study area covering parts of Toposheet nos. 72L/08, 72L/12, 73I/05 & 73I/09 belongs to Dhanbad district, Jharkhand and is bounded by A (24° 4' 8.151" N, 86° 19' 0.713" E), B (24° 4' 15.893" N, 86° 37' 10.362" E), C(23° 54' 55.795" N, 86° 18' 58.815" E) and D (23° 55' 0.041" N, 86° 37' 3.132" E).
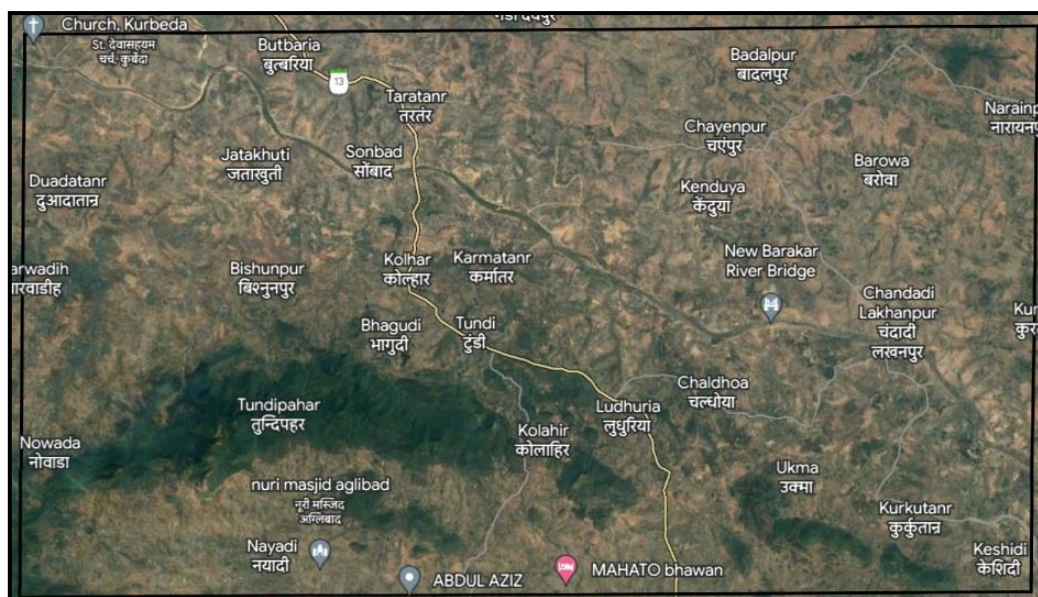
Location of the Study Area

The Precambrian Eastern Indian Shield (EIS) (Saha *et al.*, 1988; Saha, 1994; Mukhopadhyay, 2001) is characterized by complex geological and tectonic history. It consists of mainly three geological provinces- (1) Singhbhum craton characterized by Archaean TTG crust (OMTG), older (Iron Ore Group) and younger supracrustals (Singhbhum Group, Dhanjori Group) and cratonic massif of Singhbhum and Chakradharpur granite. (2) Proterozoic Fold Belt (PFB)/ North Singhbhum Mobile Belt (NSMB) and (3) Chhotanagpur Granite Gneiss complex (CGC). The Proterozoic fold belt is mainly a volcano- sedimentary assemblage of Palaeoproterozoic to Mesoproterozoic age. The northern margin of Singhbhum craton with PFB at its north is marked by prominent ductile shear zone known as Copper Belt Thrust (Dunn and Dey, 1942) or Singhbhum Shear Zone (Sarkar and Saha, 1962). Singhbhum Craton is bounded in the north by Chhotanagpur Gneiss, forming the eastern extension of the Satpura mobile belt or Central Indian Tectonic zone. The northern contact of PFB with Chhotanagpur Granite Gneiss Complex (CGC) is marked by another E-W trending ductile shear zone (Dunn and Dey, 1942; Bhattacharya, 1989), known as Tamar Porapahar Shear Zone/ South Purulia Shear Zone (SPSZ). The huge mass of CGC occurring at the north of PFB has a different tectono-metamorphic history. It is characterized by presence of different variants of granite, gneisses and granulites. A number of discrete ductile shear zones present within CGC. Among them the E-W trending brittle - ductile shear zone extending over 100 Km from Jhalda in the west through Malthol to Raghunathpur and further east to Santuri is the most significant. It is termed as North Purulia Shear Zone (NPSZ) (Prasad, 1988; Sarkar *et al.*, 1998, Sarkar, 2009, Chakraborti and Huin, 2008). In the northern part, CGC rocks are overlain by Gondwana Supergroup. The Gondwana Basins of Peninsular India contain a thick pile (~200 to 4000m) of clastic sediments preserved in graben /half-graben setting bounded by high angle normal faults Gondwana sediments are represented by a thick sequence of shallow water, fluviatile and lacustrine sediments having an aggregate thickness of about 6000-7000 m with characteristic floral-faunal content and spanning in age from Upper Carboniferous to Lower Cretaceous. It is essentially a continental succession and its upper and lower boundaries cannot be precisely defined chronostratigraphically, as floral assemblages are long-ranging and the land vertebrate remains are also sporadic in occurrence (mainly restricted to middle part of the succession). The lower and upper contacts of Gondwana sediments also do not coincide with the Standard Time Scale. This continental succession of sedimentary deposits of Southern hemisphere is unique in a way and has been informally designated as the "Gondwana Sequence".

The study area exposes rocks of Unclassified Metamorphics, Granite gneiss and migmatites belonging to Chhotanagpur Gneissic Complex, Proterozoic intrusives, e.g. metanorites and dolerites, Talchir Formation and Barakar Formation of Gondwana Supergroup.

Geological setup of the study area			
Lithology	**Formation**	**Group/Supergroup**	**Age**
Dolerite		Intrusives	Jurassic to Cretaceous
Sandstone and Shale	Barakar Formation	Gondwana Supergroup	Early Permian
Medium to fine grained sandstone, Siltstone and Splintery shale	Talchir Formation		Late Carboniferous to Early Permian
Pegmatite, Quartz vein and Meta Norite		Intrusives	Late Proterozoic
Granite Gneiss, Auguen Gneiss and Hornblende Gneiss.		Chhotanagpur Gneissic Complex	Archaean(?) to Proterozoic
Amphibolite, Hornblende gneiss, mica schist, feldspathic quartzite etc.		Unclassified Metamorphics	Archaean to Palaeo Proterozoic

(Source: compilation of TS no. 72L/12 by Shri C. Parathasarathi, Geologist)

The major part of the study area is covered by CGC and Barakar sandstone. The CGC mainly consists of different variants of granite /gneisses of composite character, porphyroclastic granite gneiss (PCG) with enclaves of metasedimentary and metabasic rocks, intrusive basic rock, and pegmatite and vein quartz. CGC is overlain by Gondwana Supergroup of rocks with a profound nonconformity in the study area. These granite- gneisses show diverse petrography and petrochemistry (Ghosh and Sengupta, 1988; Bandyopadhyay and Bandyopadhyay, 1990). Heterogeneity also exists in terms of structure and metamorphism (Pyne*et al.*, 1991). The CGC rocks mainly have undergone amphibolite grade of metamorphism, but the grade of metamorphism increases from south to north from lower amphibolite to granulite facies. CGC shows complex amalgamation of granite with Granulite facies rock in this area (Acharya, 2001, Chakraborti and Huin, 2008). In the studied area Gondwana Supergroup is represented by Barakar Formation. Barakar Formation is represented by fining upwards cycles of coarse pebbly, poorly sorted arkosic-subarkosic calcareous sandstone, siltstone, carbonaceous shale and coal. Barakar sediments show excellent primary sedimentary structures in quarry sections in the north western part. Fining upward cycles, large scale tabular cross bedding, epsilon cross bedding are indicative of meandering channel facies. Coarse to fine grained sandstones exhibiting large scale cross bedding, horizontal parallel bedding are considered to represent point bar deposits formed from lateral accretion of stream bed load on sideward migration of meandering channel (Smith, 1970). Siltstones, carbonaceous shales grading upwards into coal indicate over bank deposits. Lower Gondwana fossils such as *Glossopteris* can be seen in shales of Barakar Formation. Rock types such as granite, granite gneiss, quartz, phyllite, gabbro, dolerite (Chhotanagpur Gneissic Complex) and sandstone (Barakar formation) are noticed in the study area during field work. The trend of quartz hillocks present in the given area is in the NW-SE direction whereas the trend of granite hillocks is in the E-W direction. Barakar is the major river flowing through the study area and they are flowing in the SE direction.

2.3 Lithology
2.3.1 Unclassified Metamorphics
Unclassified Metamorphic rocks occur as linear band /bodies within gneisses and follow the regional trend of foliation and include amphibolite, hornblende schist, mica schist, feldspathic quartzite and calc-silicate rocks.

2.3.2 Chhotanagpur Gneissic Complex (CGC):
Granite gneisses are the most dominant rock types in the area. Gneisses are medium to coarse grained, which constitute the basement for the sedimentaries, to form the undulating topography of the area under consideration. Different varieties of gneisses present in the area include biotite granite gneiss, hornblendic granite gneiss and sillimanite granite gneiss and all of them are garnetiferous. Biotite granite gneiss often shows schistose character with intricate folding and crenulation. Sillimanite granite gneiss is more or less similar to biotite granite gneiss except that it contains considerable quantity of sillimanite. All these rock types are medium to coarse grained and occur mainly in the lower contours. They are structurally disturbed, tightly folded and intensely faulted.

2.3.3 Calc Granulite:
In the study area, to the south of Sangramdih, ridges of Calc granulite outcrops which are highly ferruginised and limonitised are evident. Chemogenic precipitation has occurred which resulted in a strong alteration in the outcrops. At places, iron concretions are observed.

2.3.4 Amphibolite:
Outcrops of Amphibolites occur as enclaves in the Chhotanagpur Gneissic Complex (CGC) which are devoid of alterations. Occasionally, incipient gneissosity has been observed, defined by thin alternate bands of Quartzo-feldspathic and Amphibolite-Biotite rich layers.

2.3.5 Quartzite:

On the south of Bandarchua hill slope, Quartzite boulders are exposed where boxwork vein structures are observed which are strongly ferruginised and limonitised.

2.3.6 Gondwana Super Group:

Gondwana Super Group is represented by Barakar Formation composed of sandstone, grit, shale, carbonaceous shale and coal seams. Outcrops of Buff coloured, ferruginised, fine grained, regularly sorted Sandstone along the banks of Barakar River, where porphyoblasts of Quartz are observed. These are highly matured with ferruginisation at surface. At places, grey coloured Sandstone is evident which is irregularly sorted, coarse angular grains and less matured indicating a close by provenance.

2.3.7 Intrusives:
Intrusive rocks of Proterozoic age include pegmatite, quartz vein and dolerites of Jurassic to Cretaceous age.
Dolerite

A number of dolerite dykes are seen cutting across the basin. The dolerite dyke forms a small ridge at Karitan village i.e. in the south eastern part of the Toposheet characterised by dark colour index, trending 130° sub-parallel to Barakar River.

2.4 Structures
Different structural features in the area include foliation, bedding, joints, folds and faults.
A. Foliation: It is the most common planar structure preserved in schist and gneisses.
B. Bedding: Developed in Sedimentary rocks of Gondwana Supergroup.
C. Joint: Joints are extensively developed in the area. They are strike, dip and oblique joints having steep to vertical dips. Two sets of perpendicular joints are visible in Buff Sandstone of Barakar Formation along the banks of Barakar River where bedding is prominent with cross stratification and oscillatory ripple marks. PCD, i.e. Convolute Laminations are dominant.
D. Fold: Small scale antiformal folds are developed in the schistose rocks. In the outcrops of Calc granulite, two generations of folds are observed where all the four limbs are almost sub-vertical. The first generation fold is subparallel with the regional trend of Satpura orogeny. S and Z type of folds are observed with fold interference pattern in Granite gneisses of Chhotanagpur Gneissic Complex (CGC).
E. Shear Zone: Shear zone is also noticed in granite gneiss which shows the dextral as well as sinistral sense of shearing. Some of the nala sections show the boudinage in the gneiss which were developed in the extensional regime, at few places the necking zones also present.
F. Boxwork: In the outcrops of Calc granulite, boxwork vein structures are observed which indicates that the area might have been affected by remobilisation of hydrothermal fluids.
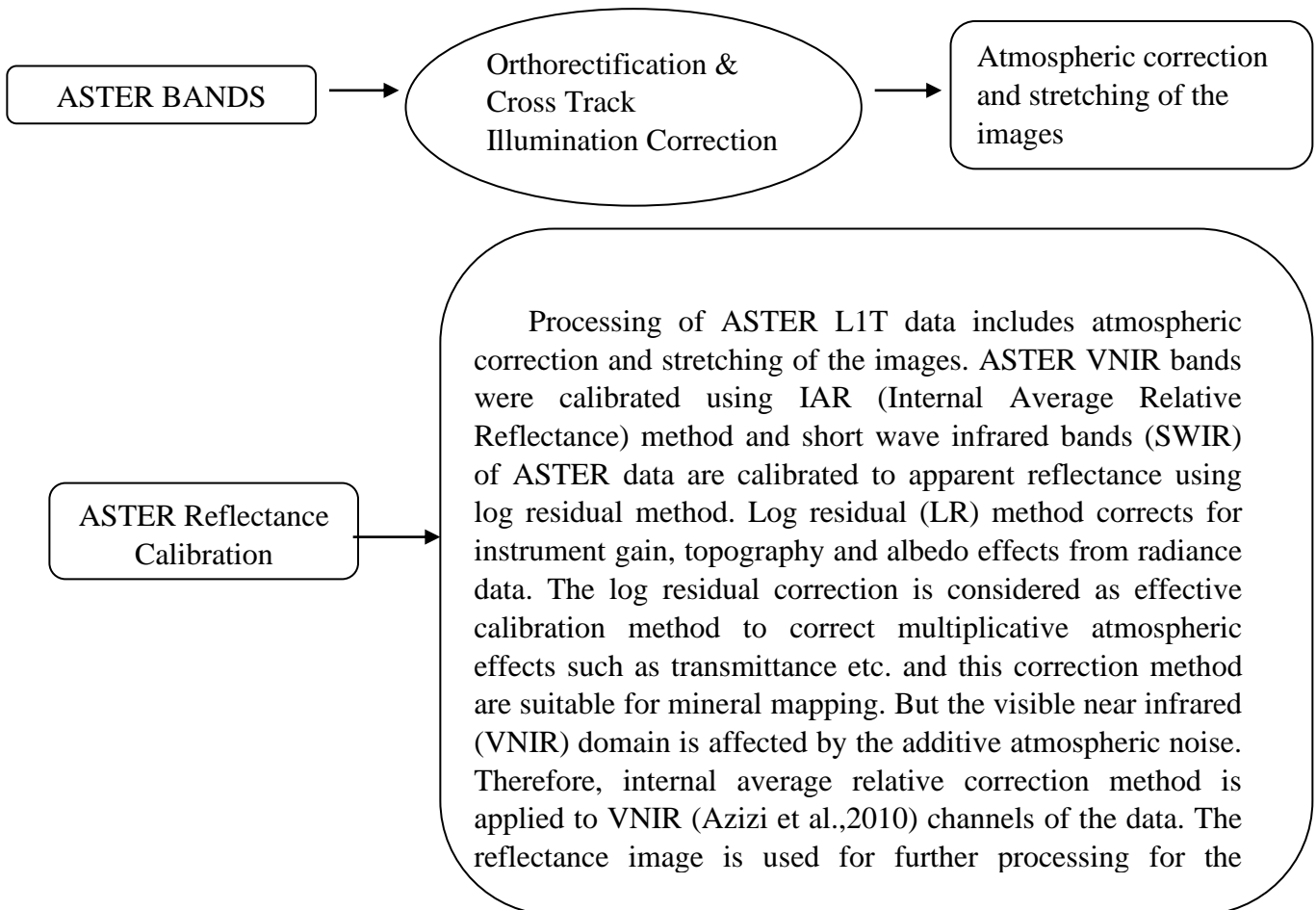
III. Materials and Methods

A cloud free Level 1B (geometric and radiometric corrected) Advanced Spaceborne Thermal Emission and Reflection Radiometer data acquired on 2007 was obtained from USGS website for the study. The data consists of 3 VNIR, 6 SWIR and 5 TIR spectral bands. The data is georeferenced in the UTM projection for theWGS-84 ellipsoid. All pre-processing of Level 1B ASTER data were carried out using ENVI 4.8 software and GIS software packages. The detailed specification of the ASTER sensor is given in Table 1. Collateral datasets such as the Geological Survey of India (GSI) district resource map (1:250000 scale) and published literature of Dhanbad district of Jharkhand was used as a geological guide to interpret and asses the image results. Due to the challenging topography and hostile conditions of the study area only few locations were visited to verify the image derived lithological map.

Table 1. ASTER sensor specification (Gomez et. al [9])

| Characteristics	VNIR	SWIR	TIR
Spectral coverage	Band 1 0.52-0.60μm Band 2 0.63-0.69μm Band 3N 0.76-0.86μm Band3B 0.76-0.86μm (N: Nadir looking) (B:Backward looking)	Band 4 1.6-1.7μm Band 5 2.145-2.185μm Band 6 2.185-2.225μm Band 7 2.235-2.285μm Band 8 2.295-2.365μm Band 9 2.36-2.43μm	nd 10 25-8.475μm nd 11 75-8.825μm nd 12 25-9.275μm nd 13 25-10.95μm nd 14 95-11.65μm
Spatial resolution (m)	15	30	90
Swath width (km)	60	60	60
Signal quantization level (bits)	8	8	12

ASTER image processing and analysis

Processing of ASTER L1T data includes atmospheric correction and stretching of the images. ASTER VNIR bands were calibrated using IAR (Internal Average Relative Reflectance) method and short wave infrared bands (SWIR) of ASTER data are calibrated to apparent reflectance using log residual method. Log residual (LR) method corrects for instrument gain, topography and albedo effects from radiance data. The log residual correction is considered as effective calibration method to correct multiplicative atmospheric effects such as transmittance etc. and this correction method are suitable for mineral mapping. But the visible near infrared (VNIR) domain is affected by the additive atmospheric noise. Therefore, internal average relative correction method is applied to VNIR (Azizi et al.,2010) channels of the data. The reflectance image is used for further processing for the

DATA PROCESSING

3.2.1. False Colour Composite (FCC):

FCC was created by applying ASTER bands 3, 2 and 1 to red (R), green(G) and blue (B) (R:G:B=3:2:1). The FCC image of the study area in ASTER data with RGB 3,2,1.
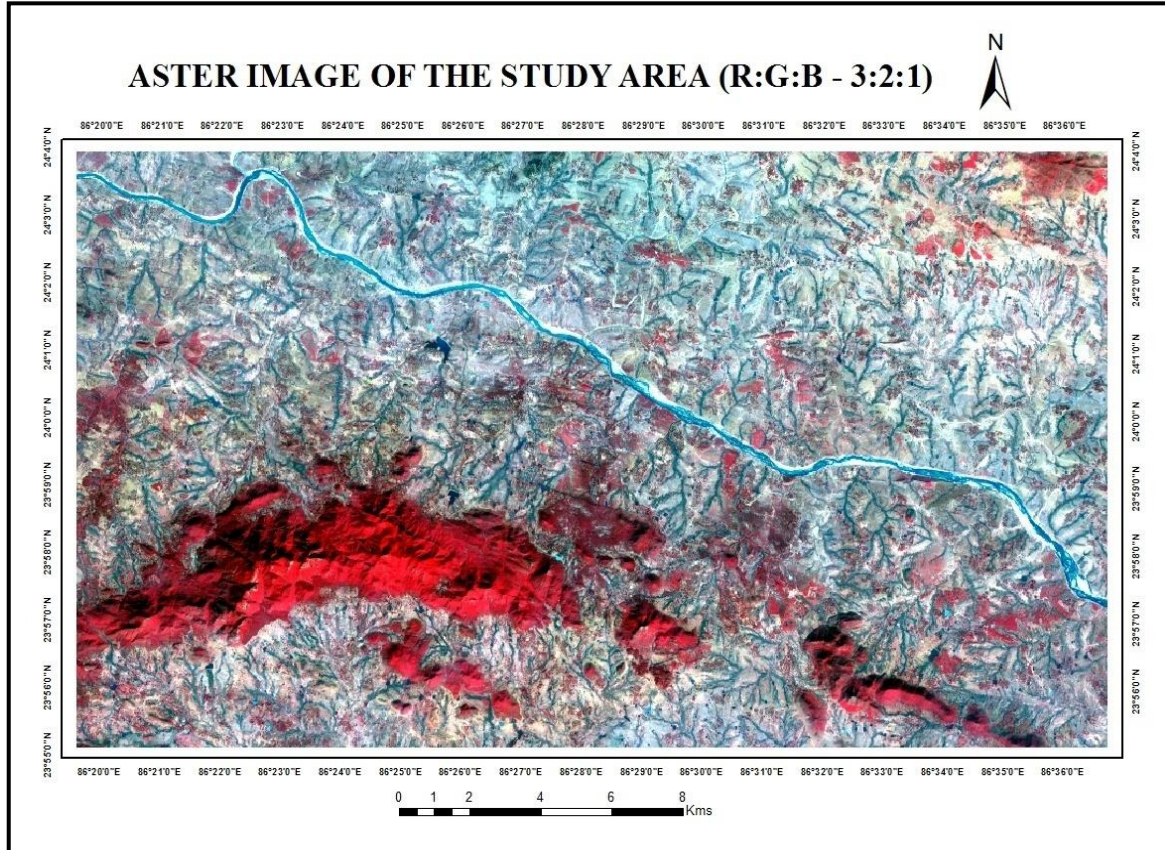
FCC of ASTER image of the Study Area (3:2:1)

3.2.2. Band Ratios:

In ASTER image, Band ratio was used to enhanced the spectral differences between band to band and reduces the topographic effect. The primary purpose of such ratios is to enhance the contrast between objects by dividing brightness values at peaks and troughs in a spectral reflectance curve. Some commonly used band ratio method for delineating, iron, carbonate, agrillic, silicates and silica alteration using ASTER multispectral data. To extract the most useful spectral information from the ASTER bands and to characterize geological features, different types of band combinations and image processing techniques are applied which includes: (1) Red-Green-Blue (RGB) band combinations, (2) band ratios and logical operations. ASTER imagery processing is a valuable tool for mapping different lithological units, hydrothermal assemblages and key ore-related hydrothermal alteration minerals. ASTER band combinations (RGB) such as 468, 321 and 731, provide a rough guide to distinguish different geological features from an area. Particularly, ASTER False-color composite 468 (RGB) images typically show argillic- and phyllic-altered rocks as red tones, and propylitic-altered rocks as green tones due to Al-O-H (centered at ASTER band 6) and Fe, MgO-H (centred at ASTER band 8) absorption features, respectively (Ali mohammad , M., et al., 2015, Mars, 2010; Tommaso and Rubinstein, 2007).

A. ARGILLIC ALTERATION (B4 +B7)/(B6 * B2)

Argillic Alteration affects mainly plagioclase feldspars and is characterized by the formation of clay minerals i.e. kaolinite and smectite group (mainly montmorillonite). It typically forms below 250°C by H^+ metasomatism and occurs on the fringes of porphyry systems. (Fig.3.4)

B. FERRIC ALTERATION (B2/B1)

Ferric alteration indicates that oxidising hydrothermal fluids percolated through the rocks. The outcrops may show high reflectance values in some of the spectral regions, and also it may absorb in some other spectral regions. Supergene altered deposits typically contain limonite, goethite, hematite and jarosite. For instance, ferric iron (hematite, goethite) absorbs in the near 0.52 μm (ASTER-B1) region and high reflectance value in the 0.63-0.69 μm (ASTER-B2) spectral range of electromagnetic radiation (EMR). The band ratio of B2/B1 of ASTER will be highlight ferric iron-rich zones.

C. PHYLLIC ALTERATION

Phyllic alteration typically forms over a wide temperature range by hydrolysis of feldspars to form sericite (fine – grained white mica), with minor association quartz, chlorite and pyrite. It is normally associated with porphyry Cu deposits, but also with mesothermal precious metal ores and volcanogenic massive sulphide deposits in felsic rocks. It is typified by the assemblage quartz-sericite-pyrite. (Fig.3.6)

## D. PROPYLYTIC ALTERATION (B7+B9)/(B8 * B2)

Propylytic alteration is a mild form of alteration representing low to intermediate temperatures (200-350°C) and low fluid/rock ratios and characterizes the margins of porphyry Cu deposits as well as epithermal. It is characterized by the addition of H_2O and CO_2 and locally S, with no appreciable H+ metasomatism. The pyrophyllite mineral show spectral absorption at 2.16 μm i.e., in-band 5 of ASTER data and its shoulder of absorption is at 2.20 μm i,e in band 6 of ASTER data. It shows reflectance in VNIR (band 4). (Fig.3.7)

## E. ADVANCED ARGILLIC ALTERATION ((B7+B9)/(B8 * B2))

General alteration represents an extreme form of base leaching where rocks have been stripped of alkali elements by very acidic fluids active in high fluid/rock ratio environments. It is characterized by kaolinite, pyrophyllite, or dickite (depending on the temperature) and alunite together with lesser quartz, topaz and tourmaline. It is commonly associated with near surface, epithermal precious metal deposits where alteration is associated with boiling fluids and condensation of volatile rich vapours to form extremely acidic solutions. (Fig.3.8)

## F. PCA (PRINCIPAL COMPONENT ANALYSIS) FOR SELECTED BANDS:

Because multispectral data bands are often highly correlated, the principal components (PC) transformation is used to produce uncorrelated output bands. This is done by finding a new set of orthogonal axes that have their origin at the data mean and that are rotated so the data variance is maximized. PC bands are linear combinations of the original spectral bands and are uncorrelated. The ASTER PCA images with high Eigenvalue loading were selected for preparation of FCC (Fig. 3.9).
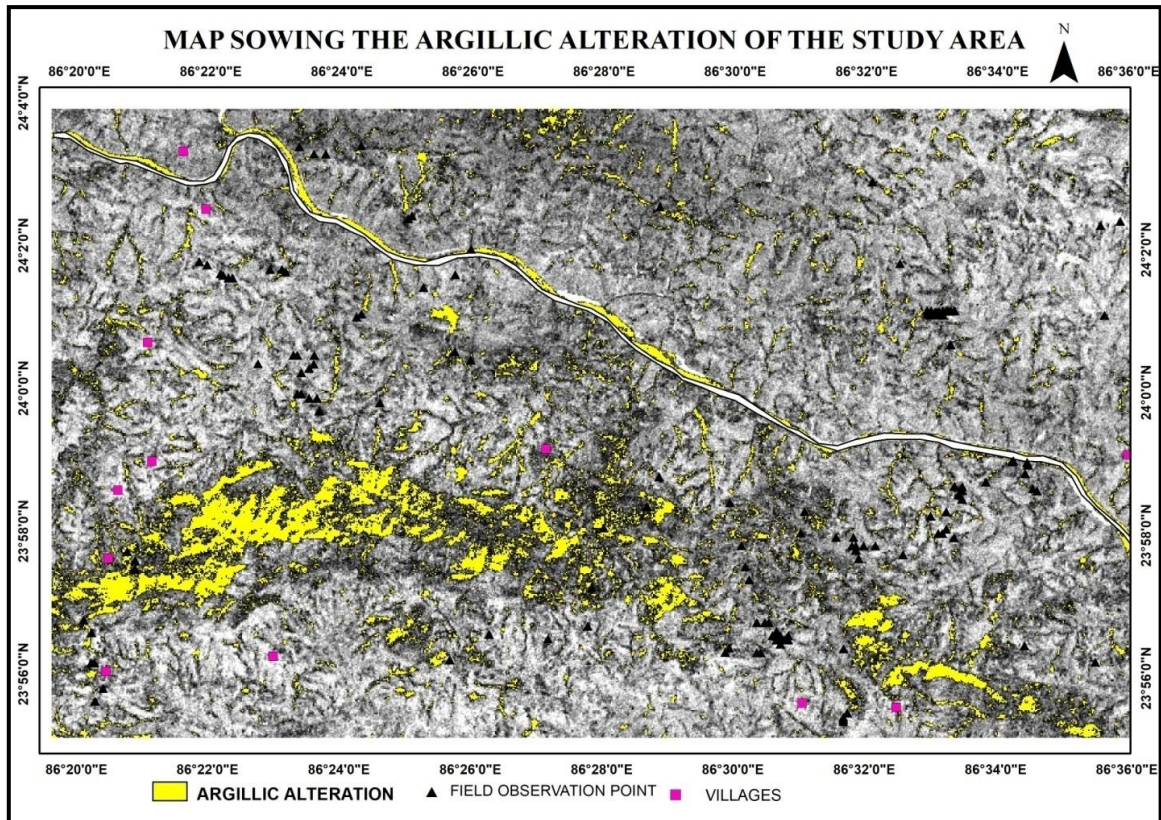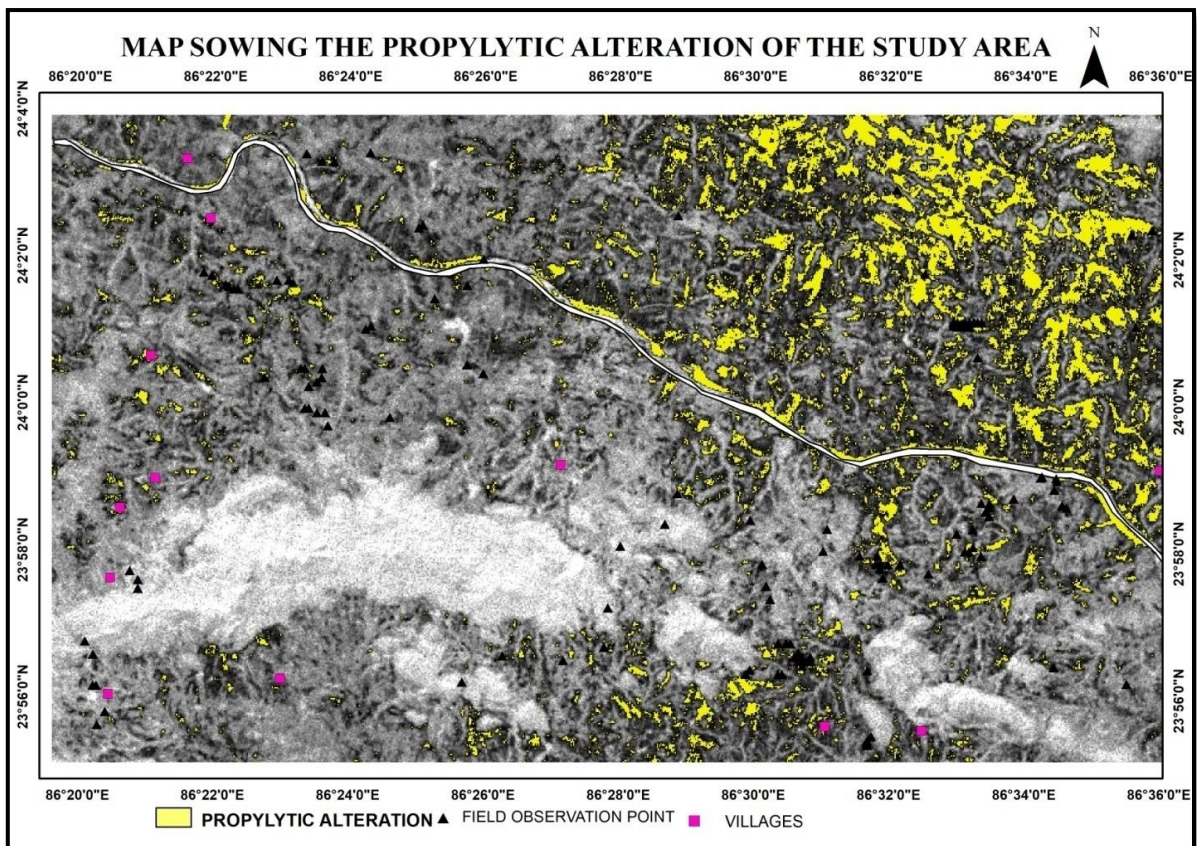
Fig. 3.4 Argillic Alteration Map of the Study Area {(B4 +B6)/B5}
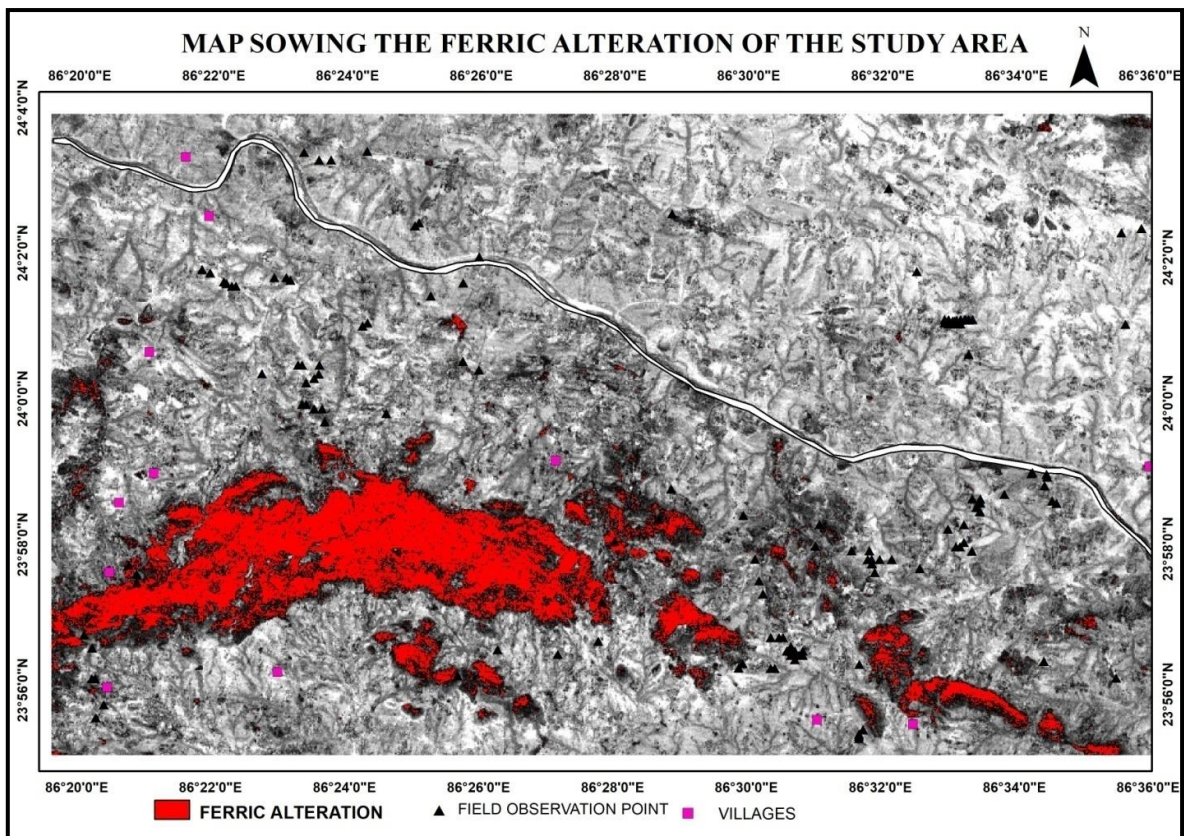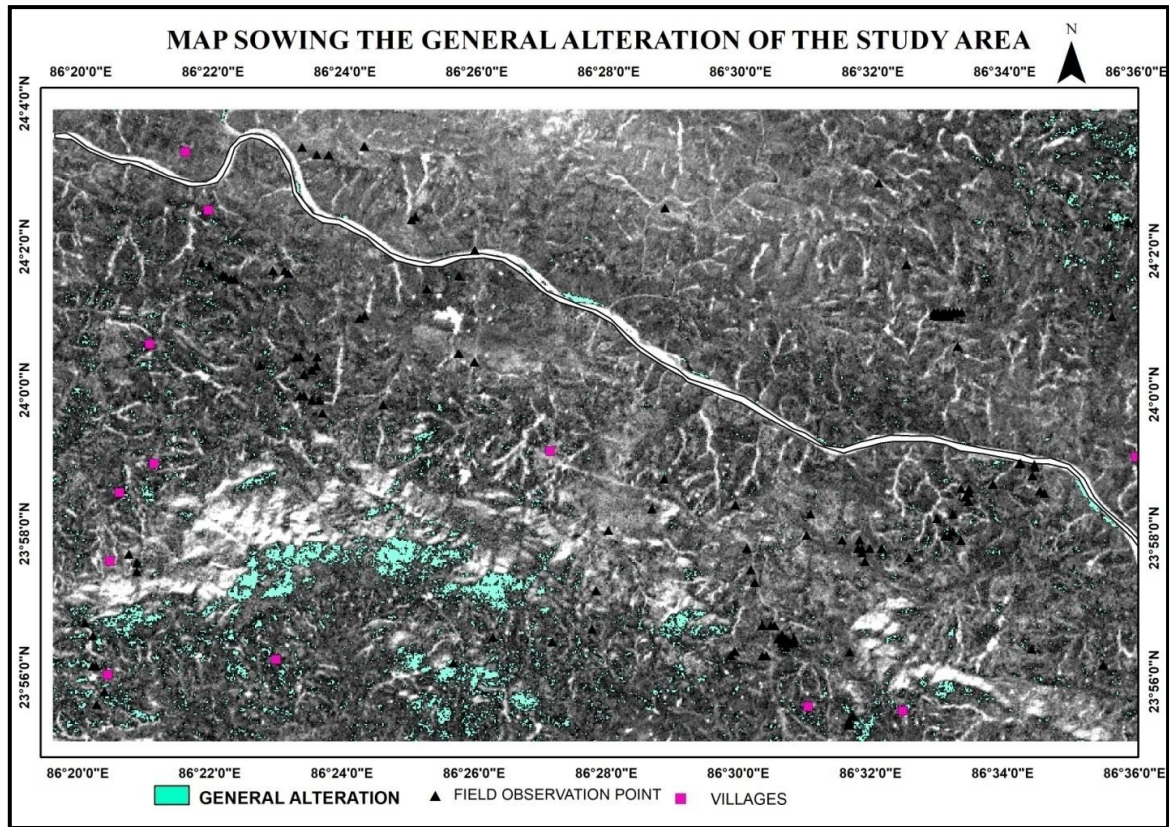

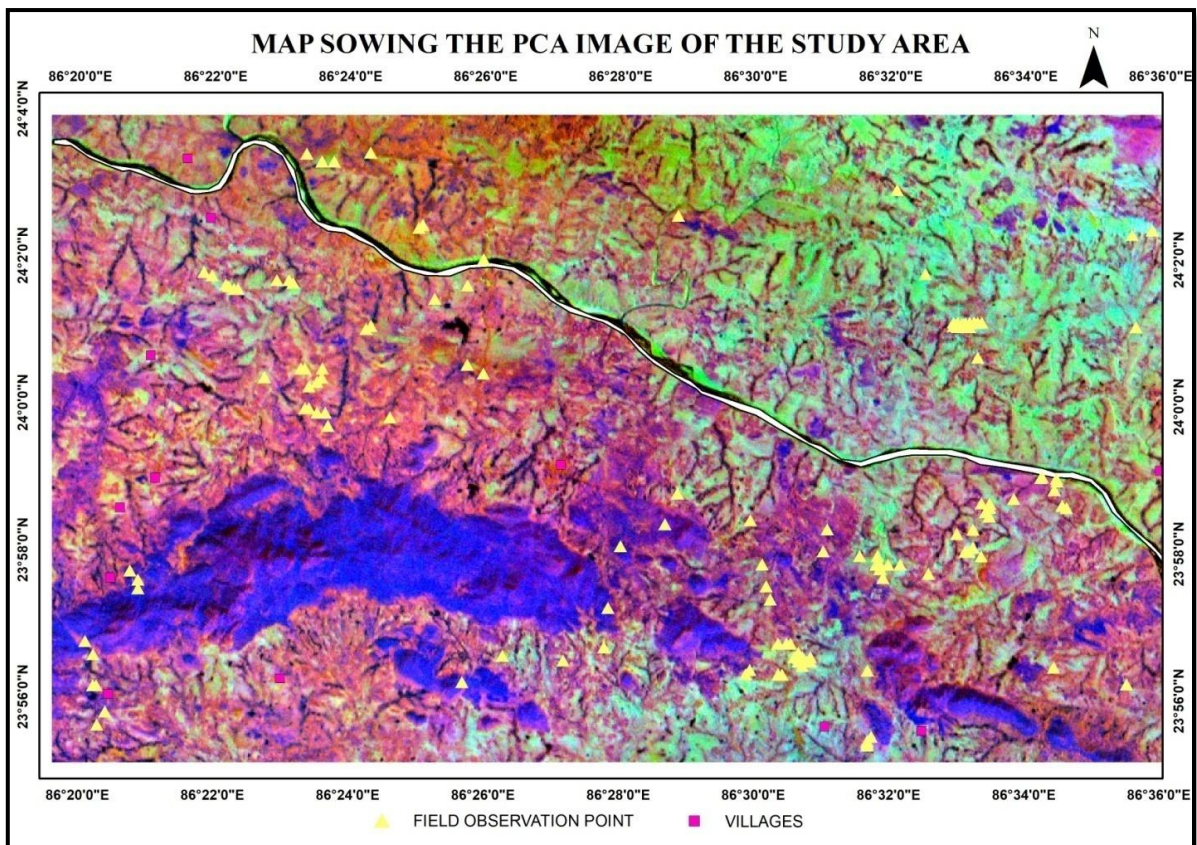**Fig. 3.5 Ferric Alteration Map of the Study Area {(B2/B1)}**
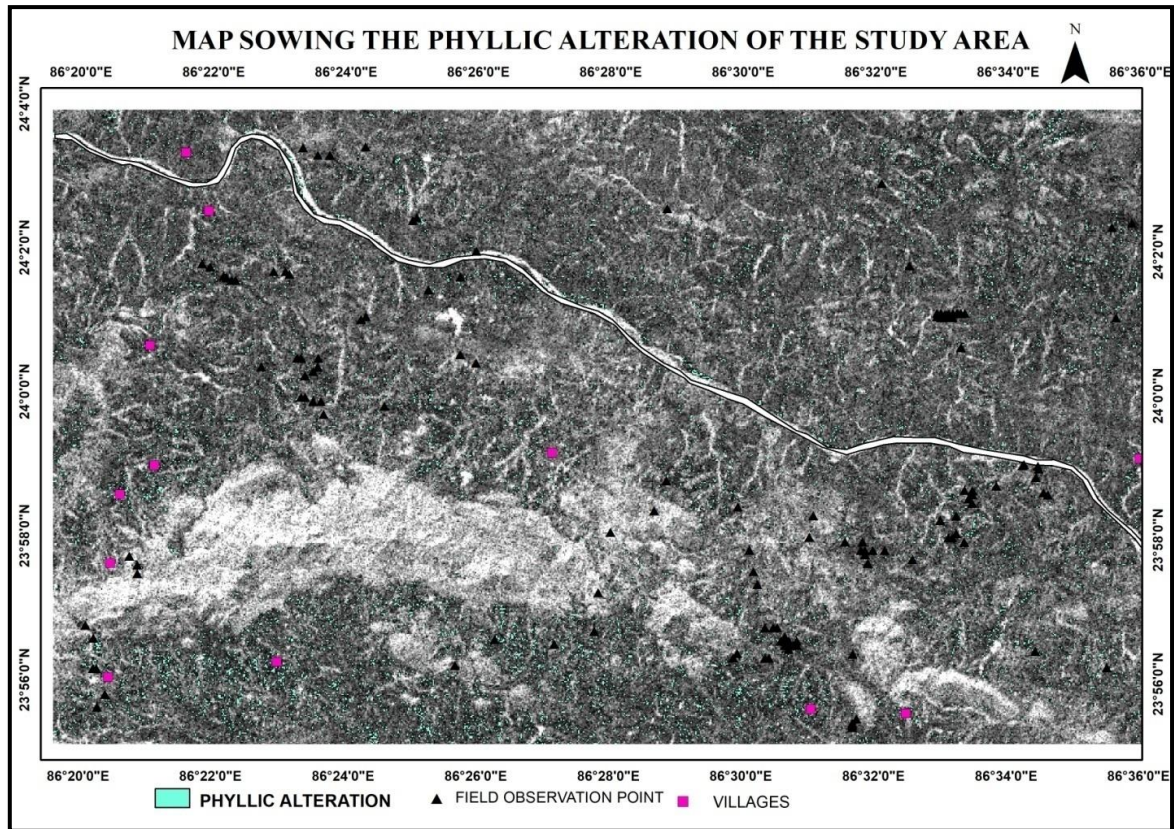
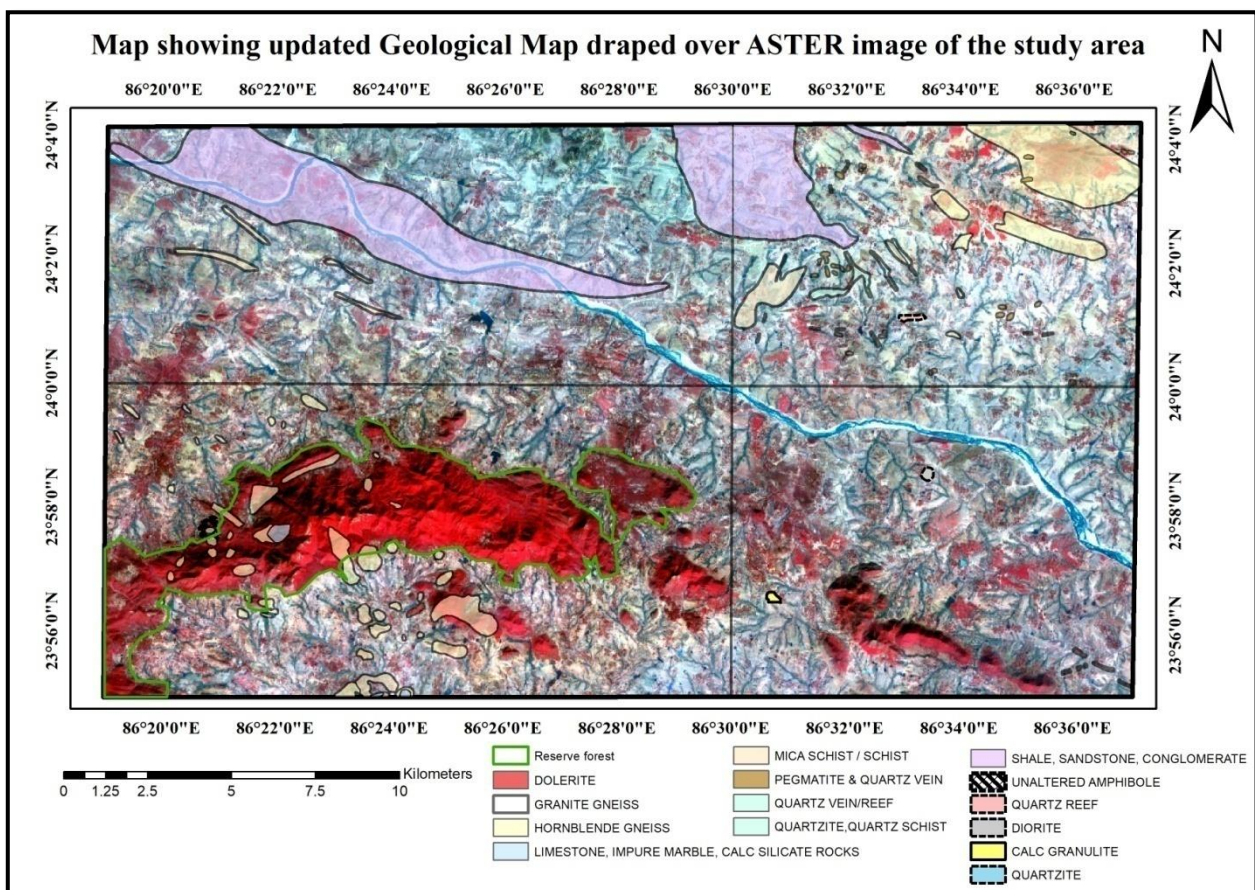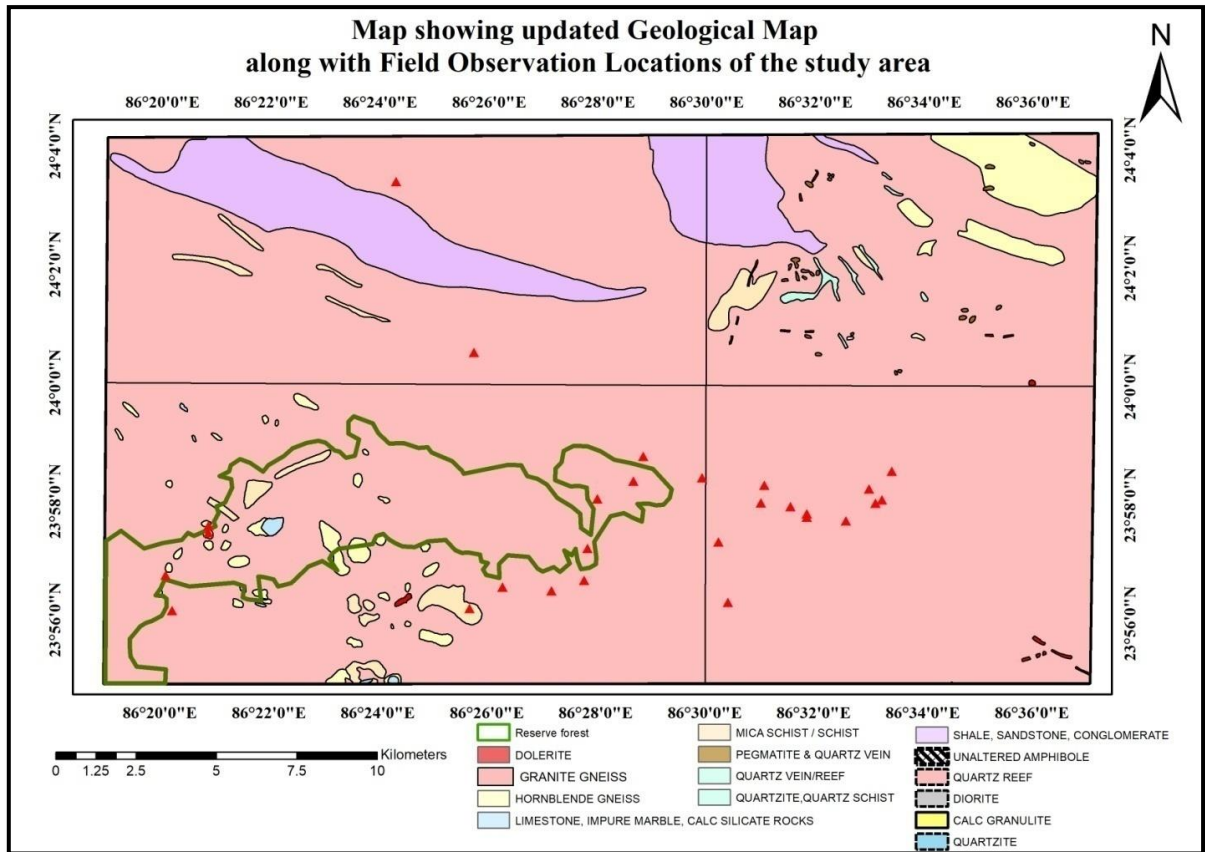**Fig.3.6 Phyllic Alteration Map of the Study Area {(B5 +B7)/B6}**

Fig. 3.7 Propylytic Alteration Map of the Study Area {(B6+B9)/(B7+B8)}

Fig.3.8 General Alteration Map of the Study Area {(B4/B5)}

Fig.3.9 PCA Image of the Study Area (534)

Map showing updated Geological Map along with Field Observation Locations of the study area

Map showing updated Geological Map draped over ASTER image of the study area

Fig. The Field Photographs of the study area during Field Investigation.
a. Outcrop of Granite gneiss, ferruginised (Loc: 23.936 86.3370)
b. Amphibolites, devoid of any alteration (Loc: 23.946 86.335)
c. Calc-granulite outcrops, showing strong ferruginisation and limonitisation (Loc: 23.943 86.511)
d. Outcrops of Calc granulite with presence of Iron Concretions (Loc: 23.942 86.513)
e. Outcrops of Granite gneiss with S & Z type of Folds (Loc: 23.936 86.337)
f. On the banks of Barakar river, Oscillatory ripple marks are observed (Loc: 24.033 86.433)

III. Conclusion

In this study, ASTER data was analyzed for identification of hydroxyl, carbonate and iron-bearing mineral phases and to map on the basis of the nature & shape of diagnostic absorption feature of mineral. The study has shown the effectiveness SWIR spectral bands of ASTER data in lithological mapping. Thus, ASTER SWIR bands coupled with the advanced image enhancement techniques are recommended as a rapid and cost effective tool for lithological discrimination and mapping in the hostile terrain of Dhanbad and other geological areas.

REFERENCES

1. Aboelkhair, H., Ninomiya, Y., Watanabe, Y., Sato, I. Processing and interpretation of ASTER TIR data for mapping of raremetal-enriched albite granitoids in the Central Eastern Desert of Egypt. Journal of African Earth Sciences 2010; 58(1): 141-151.

2. Askari, G.; Pour, A.; Pradhan, B.; Sarfi, M.; Nazemnejad, F. Band Ratios Matrix Transformation (BRMT): A Sedimentary Lithology MappingApproachUsing ASTER Satellite Sensor. Sensors 2018, 18, 3213. [PubMed]

3. Asran, A.; Emam, A.; E-Fakharani, A. Geology, structure, geochemistry and ASTER-based mapping of Neoproterozoic Gebel El-Delihimmi granites, Central Eastern Desert of Egypt. Lithos 2017, 282, 358–372.

4. Bedini, E. Mineral mapping in the Kap Simpson complex, central East Greenland, using HyMap and ASTER remote sensingdata. Advances in Space Research 2011; 47(1): 60-73.

5. Bertoldi, L.; Massironi, M.; Visona, D.; Caros, R.; Montomoli, C.; Gubert, F.; Naletto, G.; Pelizzo, M. Mapping the Buraburi granite in the Himalaya ofWestern Nepal: Remote sensing analysis in a collisional belt with vegetation cover and extreme variation of topography. Rem Sens. Environ. 2011, 115, 1129–1144.

6. Byrnes, J.; Ramsey, M.; Crown, D. Surface unit characterization of the Mauna Ulu flow field, Kilauea Volcano, Hawaii, using integrated field and remote sensing analyses. J. Volcanol. Geotherm. Res. 2004, 135, 169–193.

7. Clark, R.N. Spectroscopy of rocks, and minerals and principles of spectroscopy. In: Rencz, A.N., Ryerson, R.A. (Eds.), RemoteSensing for the Earth Sciences, Manual of Remote Sensing, 3rd ed. John Wiley & Sons 1999; New York, NY: 3–58.

8. Di Tommaso, I., Rubinstein, N. Hydrothermal alteration mapping using ASTER data in the Infiernillo porphyry deposit,Argentina. Ore Geology Reviews 2007; 32(1): 275-290.

9. El Janati, M.; Soulaimani, A.; Admou, H.; Youbi, M.; Hafid, A.; He_eran, K. Application of ASTER remote sensing data to geological mapping of basement domains in arid regions: A case study from the Central Anti-Atlas, Iguerda inlier, Morocco. Arab. J. Geosci. 2014, 7, 2407–2422.

10. Gabr, S., Ghulam, A., Kusky, T. Detecting areas of high-potential gold mineralization using ASTER data. Ore GeologyReviews 2010; 38(1): 59-69.

11. Gad, S., Kusky, T. ASTER spectral ratioing for lithological mapping in the Arabian–Nubian shield, the Neoproterozoic WadiKid area, Sinai, Egypt. Gondwana Research 2007; 11(3): 326-335.

12. Gad, S., Kusky, T. Lithological mapping in the Eastern Desert of Egypt, the Barramiya area, using Landsat thematic mapper(TM). Journal of African Earth Sciences 2006; 44(2): 196-202.

13. Galvão, L. S., Almeida-Filho, R., Vitorello, Í. Spectral discrimination of hydrothermally altered materials using ASTER shortwaveinfrared bands: Evaluation in a tropical savannah environment. International Journal of Applied Earth Observation and Geoinformation 2005; 7(2): 107-114.

14. Gomez, C., Delacourt, C., Allemand, P., Ledru, P., Wackerle, R. Using ASTER remote sensing data set for geological mapping,in Namibia. Physics and Chemistry of the Earth 2005; Parts A/B/C, 30(1): 97-108.

15. Graettinger, A.; Ellis, M.; Skilling, I.; Reata, K.; Ramsey, M.; Lee, R.; Hughes, C.; McGarvie, D. Remote sensing and geologic mapping of glaciovolcanic deposits in the region surrounding Askja (Dyngjufjoll) volcano, Iceland. Int. J. Remote Sens. 2013, 34, 7178–7198.

16. Guha, A.; Kumar, K.; Rao, E.; Parveen, R. An image processing approach for converting ASTER derived spectral maps for mapping Kolhan limestone, Jharkhand, Indian. Curr. Sci. 2014, 106, 40–49.

17. Guha, A.; Kumar, K. New ASTER derived thermal indices to delineate mineralogy of different granitoids of an Archaean Craton and analysis of their potentials with reference to Ninomiya's indices for delineating quartz and mafic minerals of granitoids—An analysis in Dharwar Craton, Indian. Ore Geol. Rev. 2016, 74, 76–87.

18. Gupta, S.N., Arora, Y.K., Mathur, R.K., Balluddin,I.Q., Prasad, B., Sahai, T.N., Sharma, S.B. Lithostatigraphic map of Aravalliregion, South-eastern Rajasthan and northern Gujrat. Geological Survey of India 1981; Hyderabad.

19. Hewson, R.D., Cudahy, T.J., Mizujiko, S., Ueda, K., Mauger, A, L. Seamless geological map generation using ASTER in theBroken Hill-Curnmona province of Australia. Remote Sensing of Environment 2005; 99: 159-172.

20. Hook, S.; Dmochowski, J.; Howard, K.; Rowan, L.; Karlstrom, K.; Stock, J. Mapping variations in weight percent silica measured from multispectral thermal infrared imagery; examples from the Hiller Mountains, Nevada, USA and Tres Virgenes-La Reforma, Baja California Sur, Mexico. Remote Sens. Environ. 2005, 95, 273–289.

21. Hosseinjani, M., Tangestani, M. H. Mapping alteration minerals using sub-pixel unmixing of ASTER data in the Sarduiyeharea, SE Kerman, Iran. International Journal of Digital Earth 2011; 4(6): 487-504.

22. Huang, Z.; Zhang, X. Lithological mapping of ophiolite composition in Zedan-Luobusha, Yarlung Zangbo suture zone using Advanced Spaceborne Thermal Emission and Reflection Radiometer (ASTER) data. Acta Petrol. Sin. 2010, 26, 3589–3596.

23. Hubbard, B.; Hooper, D.; Solano, F.; Mars, J. Determining mineralogical variations of aeolian deposits using thermal infrared emissivity and linear deconvolution methods. Aeolian Res. 2018, 30, 54–96.

24. Hyvarinen, A., E. Oja, Independent component analysis: algorithms and applications. Neural Networks 2000; vol. 13, no. 4-5:411-430.

25. Kargel, J.; Abrams, M.; Bishop, M.; Bush, A.; Hamilton, G.; Jiskoot, H.; Kaag, A.; Kie_er, H.; Lee, E.; Paul, F.; et al. Multispectral imaging contributions to global land ice measurements from space. Remote Sens. Environ. 2005, 99, 187–219.

26. Kumar, C., Shetty, A., Raval, S., Champati Ray, P.K., Sharma, R. Sub-pixel mineral mapping using EO-1 Hyperionhyperspectral data. International Archives of the Photogrammetry, Remote Sensing and Spatial Sciences 2014: XL-8: 455-461.doi: 10.5194/isprsarchives-XL-8-455-2014.

27. Li, P.; Long, X.; Liu, L. Ophiolite mapping using ASTER data: A case study of Derni ophiolite complex. Acta Petrol. Sin. 2007, 23, 1175–1180.

28. Massironi, M.; Bertoldi, L.; Calafa, P.; Visona, D. Interpretation and processing of ASTER data for geological mapping and granitoids detection in the Saghro massif (eastern Anti-Atlas, Morocco). Geosphere 2008, 4, 736–759.

29. Michael Abrams and Yasushi Yamaguchi Twenty Years of ASTER Contributions to Lithologic Mapping and Mineral Exploration; Remote Sens. 2019, 11, 1394

30. Ninomiya, Y., 2002. Mapping quartz, carbonate minerals and mafic ultramafic rocks using remotely sensed multispectral thermal infrared ASTER data. Proceedings of SPIE The International Society for Optical Engineering 4710, 191–202.

31. Ninomiya, Y.; Fu, B. Regional Lithological Mapping Using ASTER-TIR Data: Case Study for the Tibetan Plateau and the Surrounding Area. Geosciences 2016, 6, 39.

32. Ninomiya, Y.; Fu, B.; Cudahy, T. Detecting lithology with Advanced Spaceborne Thermal Emission and Reflection radiometer (ASTER) multispectral thermal infrared "radiance-at-sensor" data. Remote Sens. Environ. 2005, 99, 127–139.

33. Omran, A.; Hahn, M.; Hochschild, V.; El-Reyes, A. Lithological Mapping of Dahab Basin, South Sinai, Egypt, using ASTER Data. Photogramm. Fernerkund. Geoinform. 2012, 6, 711–726.

34. Ozkan, M.; Celik, O.; Ozyavas, A. Lithological discrimination of accretionary complex (Sivas, northern Turkey) using novel hybrid color composites and field data. J. Afr. Earth Sci. 2018, 138, 75–85.

35. Ozyavas, A. Assessment of image processing techniques and ASTER SWIR data for the delineation of evaporates and carbonate outcrops along the Salt Lake Fault, Turkey. Int. J. Remote Sens. 2016, 37, 770–781.

36. Pour, A. B., Hashim, M. Identification of hydrothermal alteration minerals for exploring of porphyry copper deposit usingASTER data, SE Iran. Journal of Asian Earth Sciences 2011; 42(6): 1309-1323.

37. Pour, A. B., Hashim, M. Identifying areas of high economic-potential copper mineralization using ASTER data in the Urumieh–Dokhtar Volcanic Belt, Iran. Advances in Space Research 2012; 49(4): 753-769.

38. Qiu, F., Abdelsalam, M., Thakkar, P. Spectral analysis of ASTER data covering part of the Neoproterozoic Allaqi-Heianisuture, Southern Egypt. Journal of African Earth Sciences 2006; 44(2): 169-180

39. Rajendran, S., Al-Khirbash, S., Pracejus, B., Nasir, S., Al-Abri, A. H., Kusky, T. M., Ghulam, A. ASTER detection of chromitebearing mineralized zones in Semail Ophiolite Massifs of the northern Oman Mountains: Exploration strategy. Ore GeologyReviews 2012; 44: 121-135.

40. Rajendran, S., Nasir, S., Kusky, T. M., Ghulam, A., Gabr, S., El-Ghali, M. A. Detection of hydrothermal mineralized zonesassociated with listwaenites in Central Oman using ASTER data. Ore Geology Reviews 2013; 53: 470-488.

41. Rajendran, S.; Hersi, O.; Al-Harthy, A.; Al-Wardi, M.; El-Ghali, M.; Al-Abri, A. Capability of Advanced Spaceborne Thermal Emission and Reflection radiometer (ASTER) on discrimination of carbonates and associated rocks and mineral identification of eastern mountain region (Saih Hatat window) of Sultanate of Oman. Carbonates Evaporates 2011, 26, 352–364.

42. Rajendran, S.; Nasir, S. ASTER spectral sensitivity of carbonate rocks—Study in Sultanate of Oman. Adv. Space Res. 2014, 53, 656–673.

43. Rajendran, S.; Nasir, S.; El-Ghali, M.; Alzebdeh, K. Spectral Signature Characterization and Remote Mapping of Oman Exotic Limestones for Industrial Rock Resource Assessment. Geosciences 2018, 8, 145.

44. Richards, J.A. Remote Sensing Digital Image Analysis: An Introduction, Springer-Verlag Berlin, Germany 1999; p.240.21. Rowan, L. C., Mars, J. C. Lithologic mapping in the Mountain Pass, California area using advanced spaceborne thermal emission and reflection radiometer (ASTER) data. Remote Sensing of Environment 2003; 84(3): 350-366.

45. Rowan, L.; Mars, J. Lithologic mapping in the Mountain Pass, California area using ASTER data. Remote Sens. Environ. 2003, 84, 350–366.

46. Rowan, L.; Mars, J.; Simpson, C. Lithologic mapping of the Mordor, NT, Australia ultramafic complex by using Advanced Spaceborne Thermal Emission and Reflection Radiometer (ASTER). Remote Sens. Environ. 2005, 99, 105–126.

47. Rowan, L.C., Hook, S.J., Abrams, M.J., Mars, J.C., 2003. Mapping hydrothermally altered rocks at Cuprite, Nevada using the Advanced Spaceborne Thermal Emissivity and Reflection Radiometer ASTER. A new satellite-imaging system. Economic Geology 98, 1019–1027.

48. Roy, A.B., Paliwal, B.S. Evolution of lower Proterozoic epicontinental deposits: stromatolite-bearing Aravalli rocks ofUdaipur, Rajasthan, India. Precamb. Res 1981; 14: 49-74.

49. Roy, S.S., Malthottra, G., Mohanty, M. Geology of Rajasthan. Bangalore: Geology Society of India 1988.

50. Sabins, F. F. Remote sensing for mineral exploration. Ore Geology Reviews 1999; 14(3): 157-183.

51. Sinha-Roy, S., Mohanty, M., Guha, D.B. Dislocation Zone in Nathdwara-Khamour Area, Udaipur district, Rajasthan and itssuignificance on the basement-cover relations in the Aravalli fold belt. Current Science 1993; 65(1): 68-72.

52. Tangestani, M. H., Jaffari, L., Vincent, R. K., Sridhar, B. M. Spectral characterization and ASTER-based lithological mappingof an ophiolite complex: A case study from Neyriz ophiolite, SW Iran. Remote Sensing of Environment 2011; 115(9): 2243-2254.

53. Tayebi, M.; Tangestani, M.; Roosta, H. Mapping salt diapirs and salt diapir-a_ected areas using MLP neural network model and ASTER data. Int. J. Dig. Earth 2013, 6, 143–157.

54. Van der Meer, F. D., Van der Werff, H. M., van Ruitenbeek, F. J., Hecker, C. A., Bakker, W. H., Noomen, M. F., &Woldai,T. Multi-and hyperspectral geologic remote sensing: A review. International Journal of Applied Earth Observation andGeoinformation 2012; 14(1): 112-128.

55. Watts, D.; Harris, N. Mapping granite and gneiss in domes along the North Himalayan antiform with ASTER SWIR band ratios. Geol. Soc. Am. Bull. 2005, 117, 879–886.

56. Yajima, T.; Yamaguchi, Y. Geological mapping of the Francistown area in northeastern Botswana by surface temperature and spectral emissivity information derived from ASTER thermal infrared data. Ore Geol. Rev. 2013, 53, 134–144.

57. Yamaguchi, Y.; Naito, C. Spectral indices for lithologic discrimination and mapping by using the ASTER SWIR bands. Int. J. Remote Sens. 2003, 24, 4311–4323.

58. Zhang, X., Pazner, M., & Duke, N. Lithologic and mineral information extraction for gold exploration using ASTER data inthe south Chocolate Mountains (California). ISPRS Journal of Photogrammetry and Remote Sensing 2007; 62(4): 271-282.

59. Zheng, S.; Fu, B. Lithological mapping of granitiods in the western Junggar from ASTER SWIR-TIR multispectral data: Case study in Karamay pluton, Xinjiang. Acta Petrol. Sin. 2013, 29, 2936–2948.

60. Zoheir, B., &Emam, A. Field and ASTER imagery data for the setting of gold mineralization in Western Allaqi–Heiani belt,Egypt: A case study from the Haimur deposit. Journal of African Earth Sciences 2014; 99: 150-164 [Original source: https://studycrumb.com/alphabetizer]